Three-dimensional seismic modelling of the crustal structure between the South Pacific and the Antarctic Peninsula

PIOTR ŚRODA

Institute of Geophysics
Polish Academy of Sciences
Ks. Janusza 64
01-452 Warszawa, Poland

Abstract   During four Polish Geodynamic Expeditions to West Antarctica between 1980 and 1991, seismic measurements were made along 21 deep refraction profiles in the Bransfield Strait and along the coastal area of Antarctic Peninsula using explosion sources. Recordings were made by 16 land stations and 8 ocean bottom seismometers. Good quality recordings were obtained up to c. 250 km distance. This allowed a detailed study of the seismic wave field and crustal structure. Three-dimensional tomographic inversion was carried out, using first arrivals from the complete dataset including off-line recordings. As a result, we obtained a 3D model of the P-wave velocity distribution in the study area. In the area adjacent to the Antarctic Peninsula coast, sedimentary cover of 0.2–3 km thickness was found, whereas in the shelf area and in the Bransfield Strait, sedimentary basins with thickness of 5–8 km were observed. In the Bransfield Strait, a high-velocity body with Vp >7.5 km/s was found at 12 km depth. The use of the off-line data allowed for determination of the horizontal extent of the body. The thickness of the crust varies from >35–40 km in the coastal area south of the Hero Fracture Zone to 30–35 km in Bransfield Strait and South Shetland Islands, and c. 15 km in the Pacific Ocean northwest of South Shetland Islands.

Keywords   Antarctic Peninsula; crustal structure; seismic modelling; seismic tomography

INTRODUCTION

Four Polish Geodynamic Expeditions to West Antarctica were organised in 1979/80, 1984/85, 1987/88 and 1990/91 by the Institute of Geophysics of the Polish Academy of Sciences. During the expeditions, seismic and geological studies in the area of the Antarctic Peninsula shelf were carried out.

Seismic refraction and wide-angle reflection measurements were made along 21 profiles along the Antarctic Peninsula between Elephant Island and Adelaide Island (Fig. 1). The purpose of the experiments was to investigate the structure and physical properties of the Earth's crust in the area of the Bransfield Strait, South Shetland Islands, Palmer Archipelago, and Adelaide Island.

More than 500 shots were fired in the sea using 50–100 kg charges of TNT, with distances between shot points of c. 5 km. Recordings were made at 16 5-channel land stations with 1 Hz vertical component seismometers. During the last expedition, eight ocean-bottom seismometers provided by Hokkaido University of Sapporo were deployed in the Bransfield Strait. Shots on several profiles were also recorded by stations located off-line. Very good recordings obtained along the profiles up to c. 250 km distance allowed a detailed study of the seismic wave field and crustal structure.

GEOLOGY AND TECTONICS

The Antarctic Peninsula is the 1500 km long peninsula separating the southeast Pacific Ocean from the Weddell Sea. The tectonic evolution of the Antarctic Peninsula was mainly affected by subduction of the oceanic crust under the Antarctic Peninsula from the Triassic up to recent times. The continental crust of the Antarctic Peninsula was thickened by magmatic and accretionary processes during the Mesozoic and Cenozoic (Garrett & Storey 1987). The recent history of subduction and associated events can be traced from the Pacific seafloor magnetic anomalies pattern. Subduction of Pacific seafloor segments has ceased progressively from southwest to northeast following oceanic ridge-trench collisions. Ridge segment boundaries are located along the major fracture zones. South of Alexander Island, the collision took place 50 m.y. ago. The subduction in the segment south of the Hero Fracture Zone stopped 6.5–4 m.y. ago. Since the last ridge-trench collision, the Antarctic Peninsula margin south of the Hero Fracture Zone has become tectonically passive. In the area between Hero and Shackleton Fracture Zones, the Drake plate is subducting under the South Shetland Islands microplate (Barker 1982). The South Shetland Islands are separated from the Antarctic Peninsula by the backarc extensional system in the Bransfield Strait, which opened later than 4 m.y. ago. The rift in the Bransfield Strait is a 15–40 km wide late Cenozoic structure along which seismic and volcanic activity is presently observed, proving that extensional processes are still active (Saunders & Tarney 1982; Pelayo & Wiens 1986).

In the study area, the Bouguer anomalies range between 20 and 140 mGal (Renner et al. 1985). The West Coast Magnetic Anomaly (WCMA—linear belt of long-wavelength positive magnetic anomalies exceeding 1000 nT), extending along the Antarctic Peninsula, has been associated with a belt of mafic rocks, 70–150 km wide and >1500 km long, intruded during the Mesozoic/Cenozoic subduction (Garrett 1990).

The results of seismic reflection experiments reveal two sedimentary basins along the Antarctic Peninsula continental shelf: the forearc basin close to the continental slope, and a second one closer to Adelaide and Anvers Islands (Anderson et al. 1990; Henriet et al. 1992). Sediments in the basins are probably composed of sandstones and mudstones of volcanic origin and glacial marine sediments (Anderson et al. 1990).
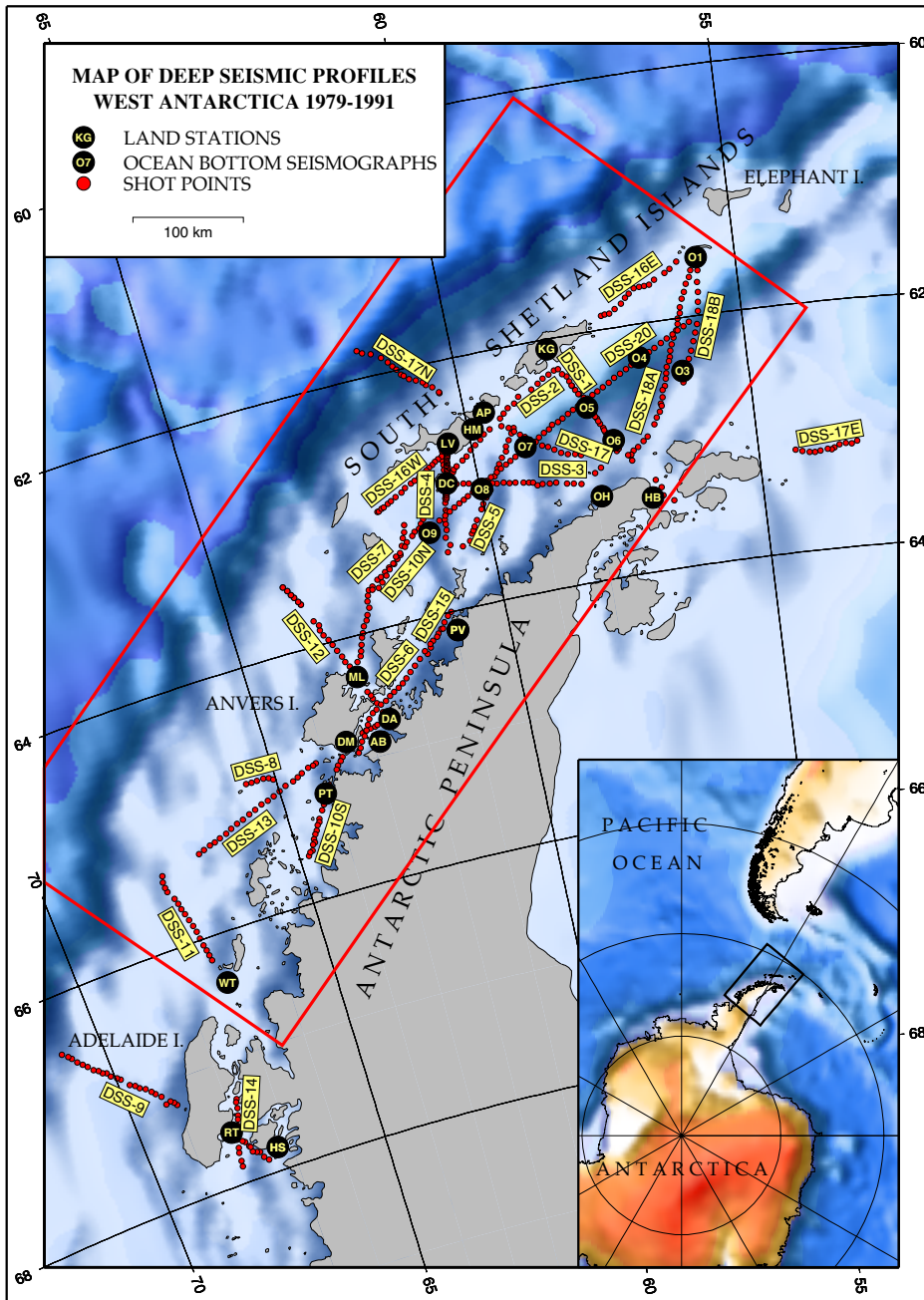
Fig. 1 Map of the study area and location of deep seismic profiles. The red frame marks the extent of the tomographic model.

More detailed discussion of geological, tectonic, and geophysical data from the region of Antarctic Peninsula can be found, for example, in papers by Dalziel & Elliot (1973, 1982), Barker & Dalziel (1983), González-Ferrán (1985), Parra et al. (1988), Birkenmajer et al. (1990), Grad et al. (1993), Środa (1994), and Środa et al. (1997).

SEISMIC DATA

The examples of the seismic data are shown on Fig. 2. Most of the sections show good quality first arrivals in the whole offset interval. In the distance interval from 80 to 170 km, reflected waves with maximum amplitudes at 120–140 km were found. They are interpreted as reflections from the Moho boundary. In this work, only first arrivals were used, due to the limitations of the method.

The seismic P-wave field shows strong differences across the study area. In the area north of the Hero Fracture Zone (the Bransfield Strait), the first arrivals show generally higher apparent velocity and higher intercept time than sections from the area south of the Hero Fracture Zone, which indicates thicker sedimentary layer and higher P-wave velocities in the middle and lower crust.

TOMOGRAPHIC INVERSION METHOD

The tomographic inversion package by Hole (1992) uses an efficient method of determining the seismic velocity distribution in a 3D medium using first arrivals. The algorithm uses an approach of linearisation of a non-linear relation between the traveltime t and the slowness $u = 1/v$. The linearisation results in an approximation:

WEST ANTARCTICA, STATION 3 (HB), PROFILE DSS−1

WEST ANTARCTICA, STATION 24 (O9), PROFILE DSS−20
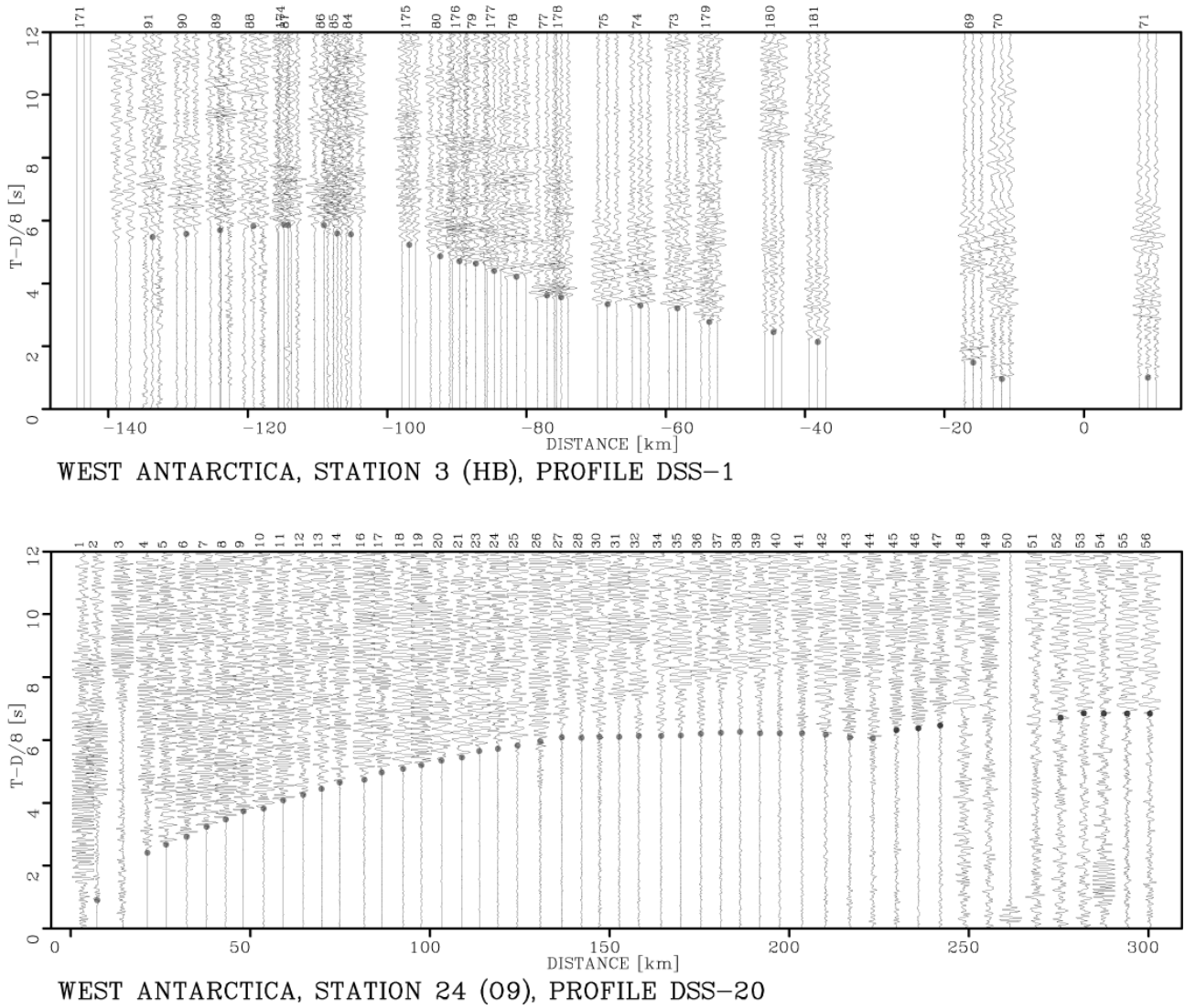
Fig. 2 Examples of the seismic record sections with picked first arrivals. Reduction velocity is 8 km/s. 2–15 Hz band-pass filter was applied.

$$\delta t = \int_{L[u_0(r)]} \delta u(r)\,dl,$$

where δt is the traveltime perturbation, δu is the slowness perturbation and u_0 is the reference slowness field. L is integration path. The solution of the above equation is found iteratively. The model of the slowness field used for inversion is parametrised using a function defined along the ray path. This leads to the following solution for the slowness perturbation:

$$\delta u(r) = \begin{cases} \delta t_j/l_j & \text{for } r \text{ along the path } j; \\ 0 & \text{otherwise.} \end{cases}$$

By summing the reference model and perturbations, we obtain a new reference model u_0. This procedure is repeated iteratively until a model with satisfying traveltime residuals is obtained.

The velocity model is defined by the rectangular grid with equidistant nodes. The traveltimes are calculated using the finite differences algorithm of Vidale (1990), adapted for media with high-velocity contrasts by Hole (1992). The

ray paths are traced from the receivers back to the source along the maximum traveltime gradient curves.

The slowness perturbation in each grid node is calculated as an average of δu in all nodes in a block around the given node. This procedure allows for the parametrisation of δu on an equidistant grid, and stabilises the inversion by smoothing the velocity field.

DATA INTERPRETATION

The purpose of this work was to make a first step in the 3D modelling of the acquired seismic data and to test if the tomographic inversion modelling of our dataset, with a rather low spatial density of recordings compared to today's standards, can produce reasonable results.

The in-line recordings were modelled in the past (e.g., Grad et al. (1993), Janik (1997a, b), Guterch et al. (1998), Środa et al. (1997)) using the 2-D raytracing package SEIS83 (Červený & Pšenčík 1983) and a procedure of iterative trial-and-error modelling. In this work, all data, including

A

B

C
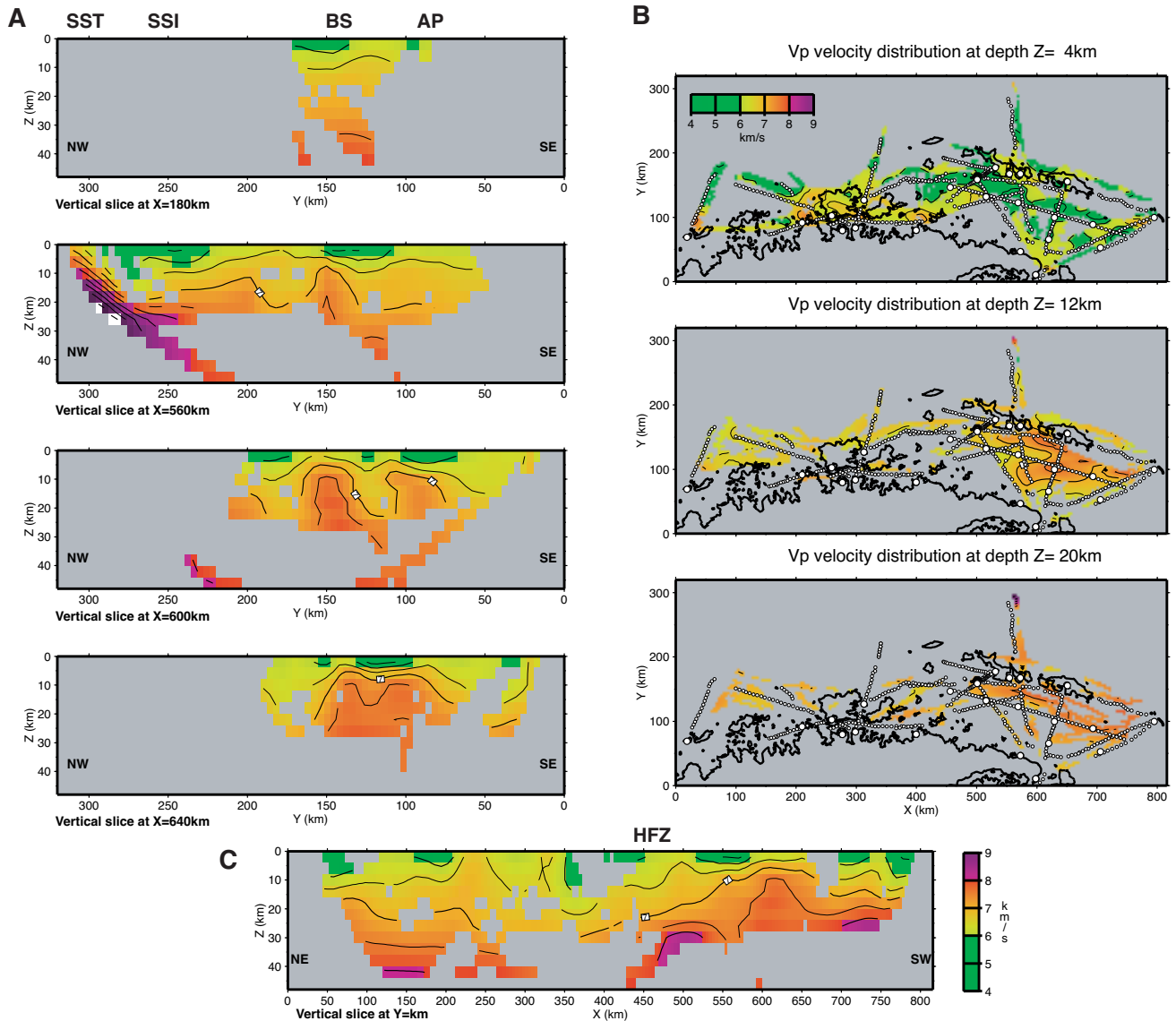
Fig. 3 *Vp* velocity distribution of the final model.   **A**, Vertical slices in the Y-Z plane.   **B**, Horizontal slices for different depths.
C, Vertical slice in the X-Z plane. Unconstrained regions (cells with zero ray density) are grey. Velocity contour interval is 0.5 km/s.

off-line recordings, were used for constructing a 3D model
of the area using the tomographic inversion package based
on the backprojection method by Hole (1992). First arrivals
of all sections were correlated and picked. Poor quality
recordings were not picked in order to avoid using false data.
The inversion program cannot accommodate bathymetry
data in the model, and so a correction for the water depth at
shotpoints has been applied to the picks, shifting the sea
bottom to the top of the model. Although the reciprocal times
checking is usually a good method of increasing the accuracy
of correlation and of rejecting doubtful picks, it could not
be applied for this kind of data with stations located off the
profiles and at different depth.

For modelling, 1642 picks of first arrivals were used.
The data were collected in the area shown in Fig. 1. The
ray coverage for the Adelaide Island area was concen-
trated only along the profiles because of lack of off-line
recordings for lines DSS-9 and DSS-14. For this reason,

the data from this area were not used. The P-wave velocity
of the model was defined in equidistant nodes in three
dimensions. The distance between nodes (the cell size)
was 4 km. The size of the model was $816 \times 320 \times 64$ km
(depth) or $204 \times 80 \times 16$ cells. Total number of cells in
the model was 261120.

In the first step of computation, picks up to 50 km offset
were used; in the next steps, this distance was increased in
order to gradually enlarge the maximum depth of the ray
penetration. This allowed constraining shallow layers first
before modelling the deeper ones. In each such step, several
iterations were nested with decreasing size of the smoothing
area. In this way the resolution of the model was gradually
increased. Several iterations were calculated in each loop.

Iterations were performed in three loops with the
following schedule:

(1) Outer loop over increasing maximum offset of picks used
    for modelling: 50, 100, 150, 250, 400 km.

Ray density at depth Z= 12km
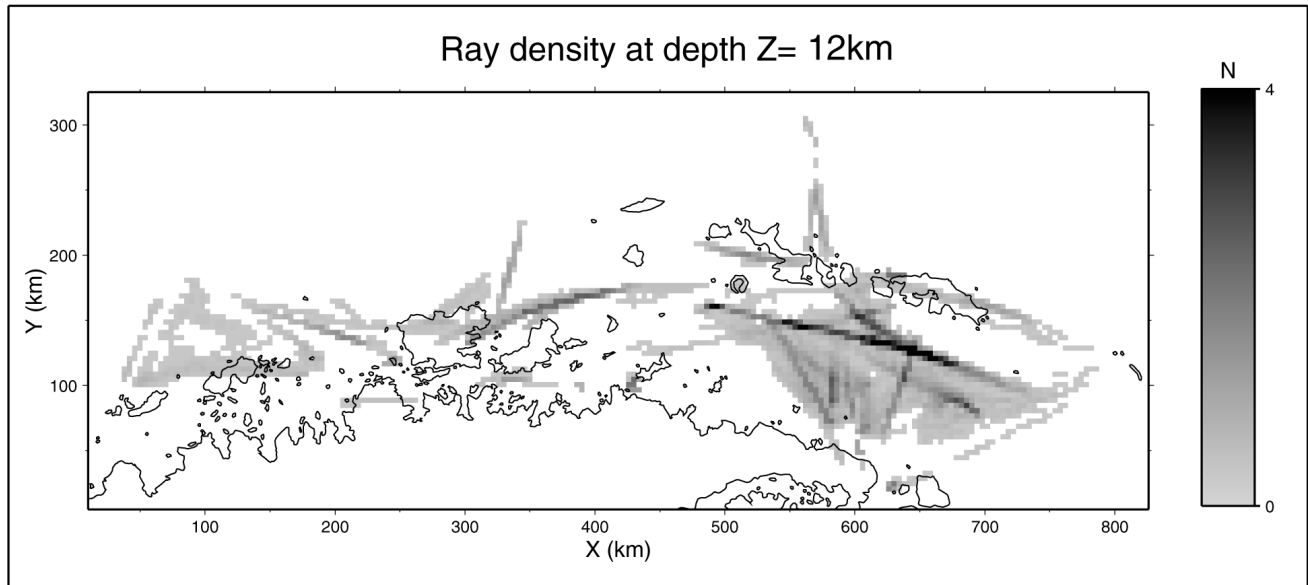
Fig. 4 Ray coverage at 12 km depth.

(2) Middle loop over decreasing moving average smoothing operator sizes: $16 \times 16 \times 6$ cells
$8 \times 8 \times 4$ cells
$4 \times 4 \times 2$ cells.

(3) Inner loop: usually five iterations with constant maximum offset and constant smoothing operator size.

The iterations in the innermost loop were stopped when the RMS curve (root mean square average of differences between experimental and calculated travel times) started to flatten, usually after 4–6 iterations. The mean RMS value for the final model was 0.24 s. The distribution of individual RMS values is approximately Gaussian-like, with most values below 0.15 s, but with several outliers, even with values up to 1 s. Relatively high mean RMS value was accepted, as lower value could not be obtained. This was probably due to the large cell size, which did not allow for detailed fitting of traveltimes, and to the fact that the reciprocity checking, which would help to remove the outliers, could not be applied.

RESULTS

The final velocity distribution is shown in Fig. 3. The final velocity model has been cut in 2D slices in selected places to show important features. For Z- (vertical) slices (Fig. 3A), the velocity value for a node was plotted only if the ray density in the corresponding cell was greater than zero in order to show only constrained areas. For X- (horizontal) slices (Fig. 3B), the ray density in the 8 cells wide swath around the cutting plane was summed to create a mask used for finding the constrained areas in the given slice.

Figure 4 shows the ray density at 12 km depth. In large parts of the constrained area, the ray density is poor (1–2 rays per cell), thus some caution is needed when interpreting the results.

In the horizontal slices, low-velocity areas with Vp < 5.0 km/s at shallow depths correspond to sediments, found previously along the Antarctic Peninsula shelf and in the

Bransfield Strait. In the area adjacent to the Antarctic Peninsula coast, sedimentary cover of 0.2–3 km thickness was found, whereas in the shelf area and in the Bransfield Strait, sedimentary basins with thicknesses of 5–8 km were observed. In the northern part of the Bransfield Strait, at depth >16 km, an area of anomalously high velocity (>7.3 km/s) was found. The vertical slice in the X-Z plane shows clearly the difference in the crustal structure between the areas south and north of the Hero Fracture Zone. A high-velocity anomaly occurs only in the Bransfield Strait, while in the area of the Palmer Archipelago south of the Hero Fracture Zone, the Vp velocity distribution is similar to normal continental crust, except for some areas of higher velocity (6.5 km/s) at shallow depth in the coastal area. In the Bransfield Strait, we observe a velocity >8.0 km/s, corresponding to the crust-mantle boundary, at 30 km depth, while the southern part is characterised by the lack of velocities over 8.0 km/s at least down to c. 40 km. The slices in the Y-Z plane show the extent of the high-velocity area and the locations of sedimentary basins in the Bransfield Strait and southwest of South Shetland Islands. The velocities over 8 km/s and inclined velocity contours in the southwestern part of the model slices may suggest shallow and dipping Moho boundary under the South Shetland Trench.

P-wave velocities over 8.0 km/s were observed only in small areas in the Bransfield Strait, where they occur at depth of c. 30 km, and under the South Shetland Trench, because the Pn phases were not found in seismic data in the southern and middle part of the study area. The use of the PmP phases would improve the model, but the current version of the software package does not allow the modelling of later arrivals.

The results of 3D tomographic modelling have been compared with previous results of Janik (1997a), who used the technique of 2D forward modelling along five intersecting profiles with the SEIS83 raytracing package (Fig. 5, 6). Comparison of raytracing models along profiles DSS-1 and DSS-20 with corresponding slices of the 3D model shows that the velocity distribution for both models

DSS-1   **DSS-20**

TOMOGRAPHIC METHOD

FORWARD MODELLING (SEIS83 RAYTRACING PACKAGE) BY JANIK (1997)
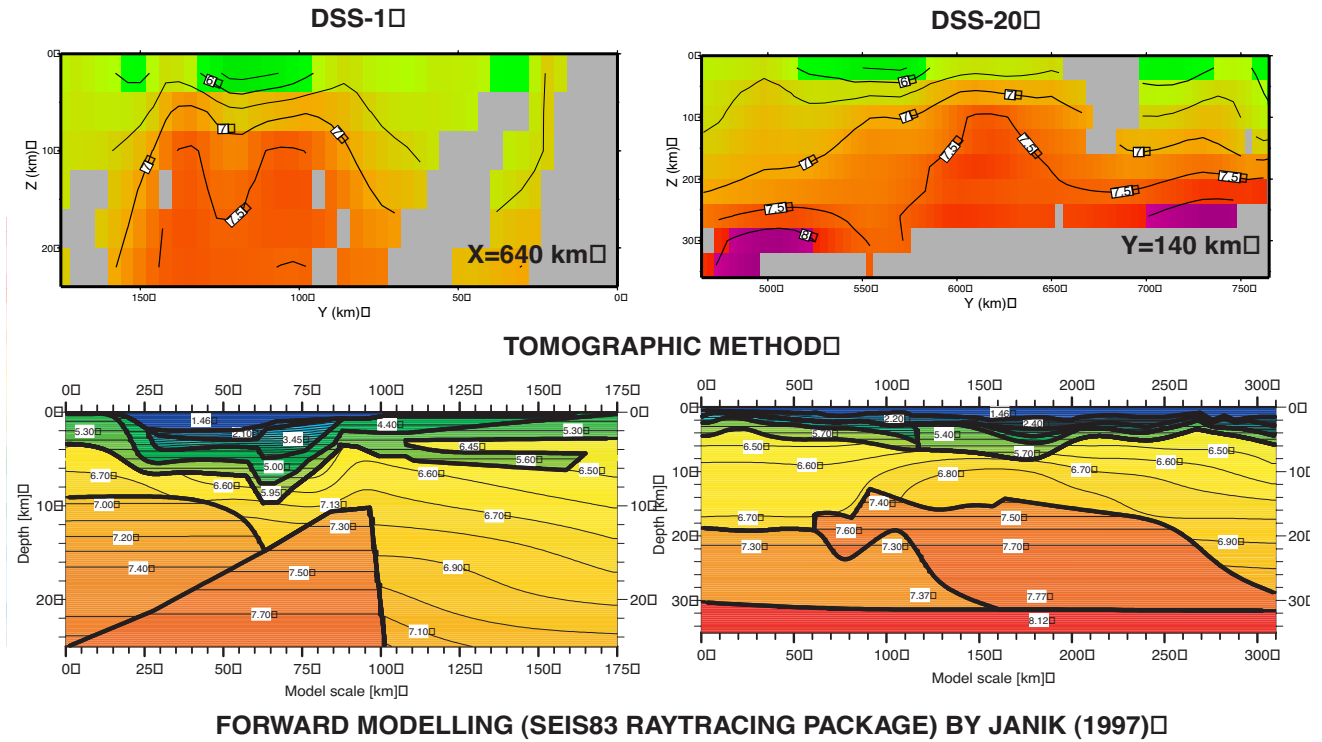
Fig. 5 Comparison of 2D models along profiles DSS-1 and DSS-20 obtained using raytracing and iterative trial-and-error forward modelling procedure (Janik 1997a), with corresponding slices of the inversion model.
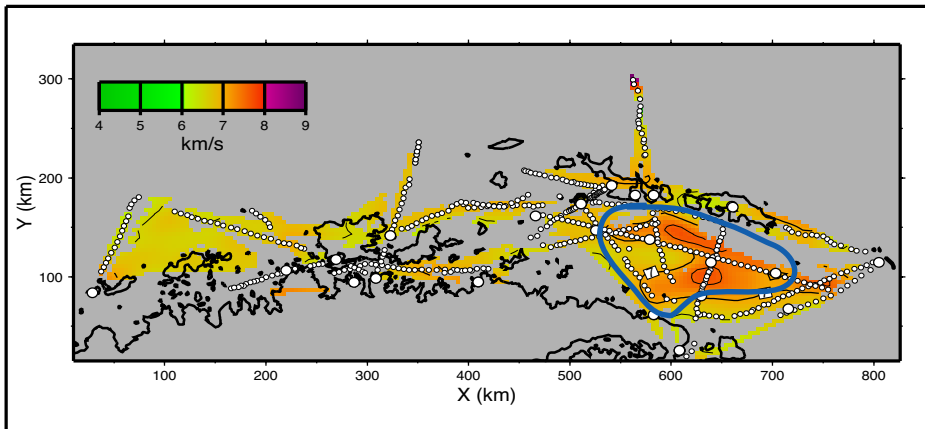
Fig. 6 Horizontal slice through the model at 12 km depth, showing the location of the high-velocity area in the Bransfield Strait. The thick blue line shows the extent of the high-velocity body as modelled by Janik (1997a).

is similar, including the locations of the sedimentary basins, the high-velocity body, and depth of the 8 km/s velocity isoline. The horizontal extent of the high-velocity area (Fig. 6) also coincides well with the one determined by Janik (1997a). Use of the complete dataset including off-line recordings allowed for a precise location of this feature. High seismic velocities in the Bransfield Strait can be explained by the existence of an ultramafic mantle material intruded into the lower crust during the crustal extension.

When comparing the results from both methods, the difference in the model parametrisation should be noted, as it affects the velocity distribution: the raytracing package SEIS83 allows definition of velocity discontinuities, while the inversion program operates on a smooth model.

CONCLUSIONS

Tomographic inversion of 1642 first arrivals produced a *Vp* velocity distrubution model up to c. 40 km depth, but at large depths the ray coverage is sparse. The geometry of this survey with its shots/stations density allows for a cell size of c. 4 km, although higher vertical resolution would be desirable.

The main features of the model are:

(1) areas with P-wave velocity <6 km/s, at depths up to 8 km, corresponding to sedimentary basins in the area of the Antarctic Peninsula shelf and in the Bransfield Strait;

(2) relatively high velocities (6.3–6.5 km/s) at depths 5–10 km in the coastal area, coinciding with location of positive magnetic anomalies (WCMA);

(3) very high *Vp* velocities (c. 7.5 km/s) at depths of 12 km in the Bransfield Strait. This confirms previous results of 2D forward modelling (Janik 1997a) and provides more information about the extent of the high-velocity area.

The information about the crustal thickness is not complete because data from reflected PmP phases were not included in the modelling. Observed Pn wave first arrivals allow for estimating crustal depth in the area south of the Bransfield Strait to >35–40 km, c. 30 km in the Bransfield Strait, and c. 15 km northwest of the South Shetland Islands. In spite of generally low ray density, the *Vp* velocity model is reasonable and is a valuable extension of the results obtained by 2D forward modelling. It is also helpful for designing the geometry of future seismic surveys in the Antarctic Peninsula area.

ACKNOWLEDGMENTS

REFERENCES

Anderson, J. B.; Pope, P. G.; Thomas, M. A. 1990: Evolution and hydrocarbon potential of the northern Antarctic Peninsula continental shelf. *In*: St John, B. *ed*. Antarctica as an exploration frontier—hydrocarbon potential, geology and hazards. *AAPG Studies in Geology 31*: 1–12.

Barker, P. F. 1982: The Cenozoic subduction of the Pacific margin of the Antarctic Peninsula: ridge crest-trench interactions. *Journal of the Geological Society, London 139*: 787–801.

Barker, P. F.; Dalziel, I. W. D. 1983: Progress in geodynamics in the Scotia Arc region. *In*: Cabré, R. *ed*. Geodynamics of the Eastern Pacific region, Caribbean and Scotia arcs. *American Geophysical Union Series 9*: 137–170.

Birkenmajer, K.; Guterch, A.; Grad, M.; Janik, T.; Perchuć, E. 1990: Lithospheric transect Antarctic Peninsula – South Shetland Islands, West Antarctica. *Polish Polar Research 11*: 241–258.

Červený, V.; Pšenčík, I. 1983: Program SEIS83, numerical modelling of seismic wave fields in 2-D laterally varying layered structures by the ray method (software package). Prague, Charles University.

Dalziel, I. W. D.; Elliot, D. H. 1973: The Scotia arc and Antarctic margin. *In*: Narin, A. E. M.; Stehli, F. G. *ed*. The ocean basins and margins (the South Atlantic). New York and London, Plenum Press. Pp. 171–246.

Dalziel, I. W. D.; Elliot, D. H. 1982: West Antarctica: problem child of Gondwanaland. *Tectonics 1*: 3–19.

Garrett, S. W. 1990: Interpretation of reconnaissance gravity and aeromagnetic surveys of the Antarctic Peninsula. *Journal of Geophysical Research 95*: 6759–6777.

Garrett, S. W.; Storey, B. C. 1987: Lithospheric extension on the Antarctic Peninsula during Cenozoic subduction. *In*: Coward, M. P.; Dewey, J. F.; Hancock, P. L. *ed*. Continental extensional tectonics. *Geological Society Special Publication 28*: 419–431.

González-Ferrán, C. 1985: Volcanic and tectonic evolution of the northern Antarctic Peninsula—late Cenozoic to Recent. *In*: Husebye, E. S.; Johnson, G. L.; Kristoffersen, Y. *ed*. Geophysics of the polar regions. *Tectonophysics 114*: 389–409.

Grad, M.; Guterch, A.; Janik, T. 1993: Seismic structure of the lithosphere across the zone of subducted Drake plate under the Antarctic plate, West Antarctica. *Geophysical Journal International 115*: 586–600.

Guterch, A.; Grad, M.; Janik, T.; Środa, P. 1998: Polish Geodynamic Expeditions—seismic structure of West Antarctica. *Polish Polar Research 19*: 113–123.

Henriet, J. P.; Meissner, R.; Miller, H.; the GRAPE Team 1992: Active margin along the Antarctic Peninsula. *In*: Shimamura, H.; Hirn, A.; Makris, J. *ed*. Detailed structure and processes of active margins. *Tectonophysics 201*: 229–253.

Hole, J. A. 1992: Nonlinear high resolution three-dimensional seismic travel time tomography. *Journal of Geophysical Research 97*: 6553–6562.

Janik, T. 1997a: Seismic crustal structure of the Bransfield Strait, West Antarctica. *Polish Polar Research 18*: 171–225.

Janik, T. 1997b: Seismic crustal structure in the transition zone between Antarctic Peninsula and South Shetland Islands. *In*: Ricci, C. A. *ed*. The Antarctic region: geological evolution and processes. Siena, Terra Antartica Publication. Pp. 679–684.

Parra, J. C.; Yáñez, G.; Grupo de Trabajo USAC 1988: Aeromagnetic survey on the Antarctic Peninsula and surrounding seas: integration of the data obtained at different altitudes. *Ser. Cient. INACH 38*: 117–131.

Pelayo, A. M.; Wiens, D. A. 1986: Seismotectonics of the western Scotia Sea region (abstract). *EOS Transactions or the American Geophysical Union 67 (44)*: 1239.

Renner, R. G. B.; Sturgeon, L. J. S.; Garrett, S. W. 1985: Reconnaissance gravity and aeromagnetic surveys of the Antarctic Peninsula. *British Antarctic Survey Scientific Report 110*.

Saunders, A. D.; Tarney, J. 1982: Igneous activity in the southern Andes and northern Antarctic Peninsula: a review. *Journal of the Geological Society, London 139*: 691–700.

Środa, P. 1994: Seismic modelling of the Earth's crust structure in the area of the Adelaide Island and Palmer Archipelago, West Antarctica. *In*: Zalewski, S. M. *ed*. XXI Polar Symposium, 23–24 September, Warsaw. Pp. 81–86.

Środa, P.; Grad, M.; Guterch, A. 1997: Seismic models of the Earth's crustal structure between the South Pacific and the Antarctic Peninsula. *In*: Ricci, C. A. *ed*. The Antarctic region: geological evolution and processes. Siena, Terra Antartica Publication. Pp. 685–689.

Vidale, J. E. 1990: Finite-difference calculation of travel times in three dimensions. *Geophysics 55*: 521–526.

Wessel, P.; Smith, W. H. F. 1998: New, improved version of Generic Mapping Tools released. *EOS Transactions of the American Geophysical Union 79 (47)*: 579.